GEOLOGIJA *65/2*, 161–175, Ljubljana 2022
https://doi.org/10.5474/geologija.2022.010

Composite landslide in the dynamic alpine conditions: a case study of Urbas landslide

Sestavljeni plaz v dinamičnih alpiskih razmerah: primer plazu Urbas

Ela ŠEGINA, Mateja JEMEC AUFLIČ, Matija ZUPAN, Jernej JEŽ & Tina PETERNEL

Geological Survey of Slovenia, Dimičeva ulica 14, SI-1000 Ljubljana, Slovenia; e-mail: ela.segina@geo-zs.si, mateja.jemec@geo-zs.si, matija.zupan@geo-zs.si, jernej.jez@geo-zs.si, tina.peternel@geo-zs.si

Prejeto / Received 27. 5. 2022; Sprejeto / Accepted 12. 10. 2022; Objavljeno na spletu / Published online 12. 12. 2022

Key words: composite landslide, alpine conditions, kinematics, monitoring, sediment discharge
Ključne besede: sestavljeni plaz, alpske razmere, kinematika, monitoring, prehajanje sedimenta

Abstract

The alpine environment is characterized by complex geology, high-energy terrain, deeply incised river valleys with high erosional potential, extreme weather conditions and dynamic geomorphic processes. Such settings provide favourable conditions for the formation of composite landslides rather than individual slope mass movement phenomena. As an example, we present the kinematics of the composite landslide Urbas in the North of Slovenia which developed in the complex geological and morphological settings characteristic of the alpine environment. The research combines several monitoring techniques and involves the integration of both surface and subsurface displacements measured in the landslide area. The results indicate that the composite sliding process consists of several simultaneous and interrelated types of movements occurring in different segments of the unstable mass that are governed by different mechanisms of displacements, such as rockfall, sliding and debris flow. The kinematic characteristics of a deep-seated landslide that formed in such conditions vary spatially, but is rather homogenuous vertically, indicating translational type of movement. Spatial kinematic heterogeneity is primarily related to the diverse terrain topography, reflecting in different displacement trends. Based on the revealed kinematic proprieties of the sliding material, the sediment discharge illustrates the sliding material balance which estimates the volume of the retaining material that represents the potential for slope mass movement events of larger scales.

Izvleček

Za alpsko okolje so značilni kompleksna geologija, razčlenjeno površje, globoko vrezane rečne doline z visokim erozijskim potencialom, ekstremne vremenske razmere in dinamični geomorfni procesi. Takšne razmere so, bolj kakor za nastanek posameznih pojavov pobočnih premikov, prikladne za razvoj sestavljenih plazov. Kot primer takšnega pojava predstavljamo primer sestavljenega plazu Urbas, ki se nahaja v severnem delu Slovenije in je nastal v zapletenih geoloških in morfoloških razmerah značilnih za alpsko okolje. V raziskavi združujemo več tehnik spremljanja plazov in povezujemo izmerjene površinske premike in premike na območju drsne ploskve. Rezultati kažejo, da proces sestavljenega plazenja vključuje več medsebojno povezanih tipov premikov, ki se, z različnimi mehanizmi premikanja (podor, plazenje, drobirski tok), istočasno odvijajo v različnih delih premikajoče se gmote. Kinematične značilnosti globokega plazu, ki je nastal v takšnih razmerah, se spreminjajo prostorsko, po globini pa so precej homogene, kar nakazuje na translacijski tip premikanja plazu. Prostorska kinematična heterogenost pa je v prvi vrsti posledica oblikovanosti površja, ki se odraža v različnih hitrostih premikov. Na podlagi ugotovljenih kinematičnih lastnosti plazečega materiala smo s pomočjo računanja prehajanja sedimenta ponazorili bilanco plazeče se mase in ocenili prostornino materiala, ki zastaja na območju plazu in ki predstavlja potencial za pojav pobočnih masnih premikov večjih razsežnosti.

Introduction

The alpine environment is generally characterized by complex geology, high-energy terrain, steep rocky slopes, deeply incised river valleys with high erosional potential, extreme weather conditions and dynamic geomorphic processes. Such conditions are favourable for the formation of slope mass movements of different types and sizes, from large-scale deep-seated rotational and translational slides to shallow landslides, slumps and sediment gravity flows in the form of debris flows or mudflows. Rather than individual slope mass movements, such complex conditions commonly result in the formation of landslides, characterized by several types of movements that act simultaneously in different parts of the sliding mass.

While complex landslides are slope mass movements with a combination of two or more principal types of movement in a sequence (Varnes, 1978), the composite landslides exhibit at least two types of movements simultaneously in different segments of the failing mass (Cruden & Varnes, 1993).

The main challenge in investigating the composite landslides is in capturing the complete landslide area, which may consist of several different geomorphological features and could be driven by different geomorphic processes. For example, steep rocky mountain peaks with rockfall areas in the hinterland of the deep-seated landslide could provide supplementary input material and impact the main sliding process along the sliding surface with an additional load. Also, the sliding material originating from the deep-seated landslide could supply the debris-flow channel. Different processes involved in the composite landslides demand different monitoring techniques that considerably worsen the data comparison. Heterogeneous geomechanical characteristics of the sliding material, common for composite landslides in complex geological conditions, also need to be considered as an important factor. For this reason, landslide body kinematics needs to be analysed in three dimensions, as surface displacements may not adequately represent the displacements occurring at depth.

Landslide kinematics is a common topic in the modern landslide research (Baum et al., 1993; Coe et al., Brückl et al., 2006; Baldi et al., 2008; Mackey et al., 2009; Uzielli et al., 2015; Schlögel et al., 2015b; Gullà et al., 2016; Schulz et al., 2012, 2017; Frattini et al., 2018; Crippa & Agliardi, 2021). Also, several landslides in the alpine environment have already been analysed and presented from different perspectives (Crosta et al., 2004; Mikoš et al., 2006; Boniello et al., 2010; Barth 2013; Hussin et al., 2015; Schlögel et al., 2015a; Viganò et al., 2021; Jemec Auflič et al., 2017; Mikoš 2020, 2021 etc.). Although natural conditions are rather commonly characterized by complex geological and morphological settings, the kinematic or other analysis of composed landslides remains a rare topic in landslide research (Stumvoll et al., 2022).

The contribution of the present paper to the scientific community is to expose the phenomenon of composite land sliding, present the applicable methodological approaches and give an example of the composite landslide kinematics that develops in the complex alpine conditions.

Study area

The composite landslide Urbas is located in the Karawanks mountain ridge in the eastern part of the Alps (Fig. 1) and extends between the elevations of 1150 m at the toe and 1350 m at the crown. The area is under the influence of the alpine climate, characterized by an annual precipitations between 2000 and 2600 mm with the primary precipitation peak in autumn and secondary in the spring, and usually 150–200 days of snow cover per year (Slovenian Environment Agency).

In the last decades, several site investigations and monitoring projects have been carried out in the wider landslide-prone area (Mikoš et al., 2008; Jež et al., 2008; Komac et al., 2014; Oven et al., 2019; Peternel et al., 2018; Janža et al., 2018; Jemec Auflič et al., 2019; Šegina et al., 2020). For a detailed overview of the investigations see Peternel et al. (2022). Several landslide bodies were identified, among which the composite landslide Urbas is the largest phenomenon in the area (Peternel et al., 2018) (Fig. 1). It covers an area of about 1 km^2. Like some other slope instabilities in the area (Peternel et al., 2018), its occurrence is tightly connected to the complex geological settings of the Karawanks system (Fodor et al., 1998; Jež et al., 2008).

Spatially limited deep-seated sliding formed within the Košuta fault zone in a several hundred meters wide area of soft, tectonically deformed Palaeozoic clastic rocks with low permeability (siltstone and claystone predominate, while sandstone and conglomerate appear in subordinate quantities) that stretches along the Karawanks in the central part of the slope (Fig. 2a). An estimated volume of the deep-seated landslide body is 1.578.700 m^3. A sliding surface was determined at the depth of down to 29.9 m (Fig. 2b).

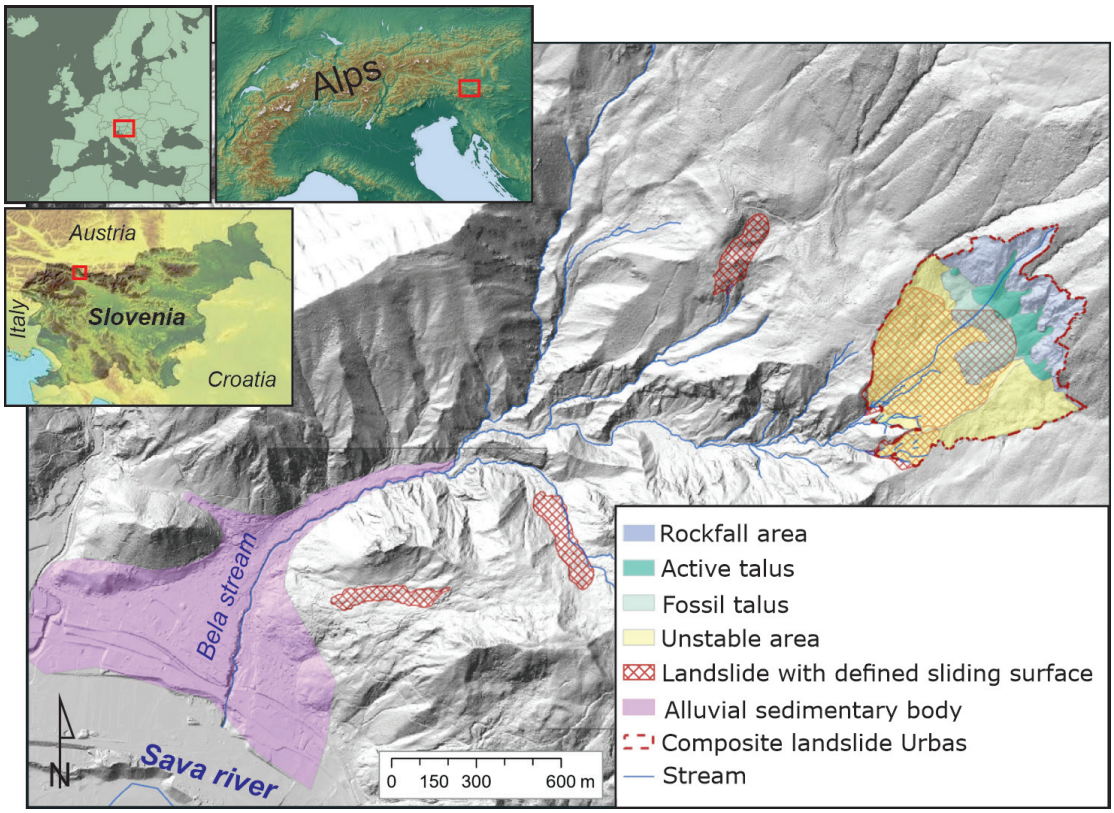

Fig 1. Location and main elements of the composite landslide Urbas.

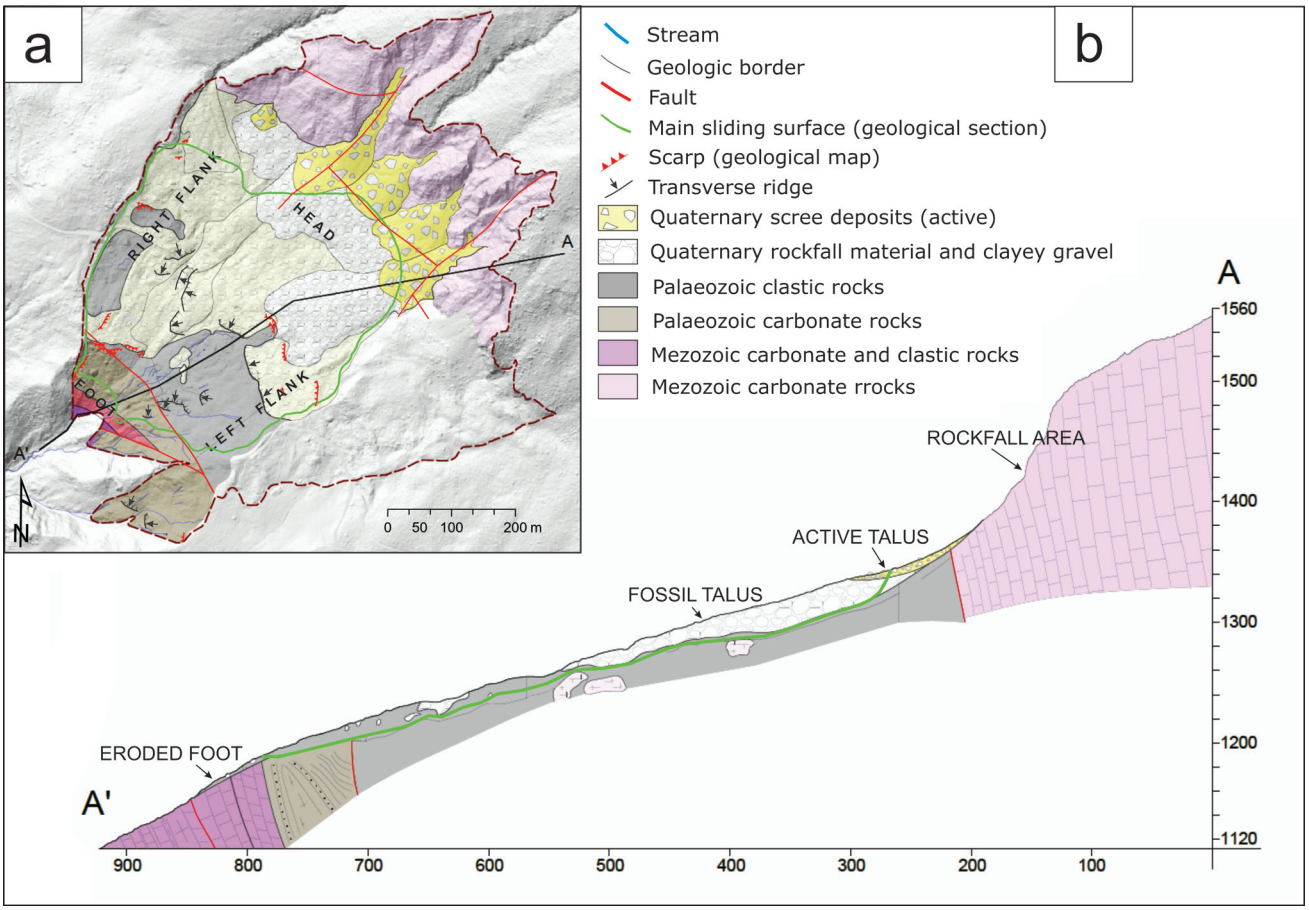

Fig. 2. a – Geological settings of the Urbas landslide, b – Geological section of the Urbas landslide (modified after Šegina et al., 2020). The SKUA-GOCAD software was used to obtain the main sliding surface.

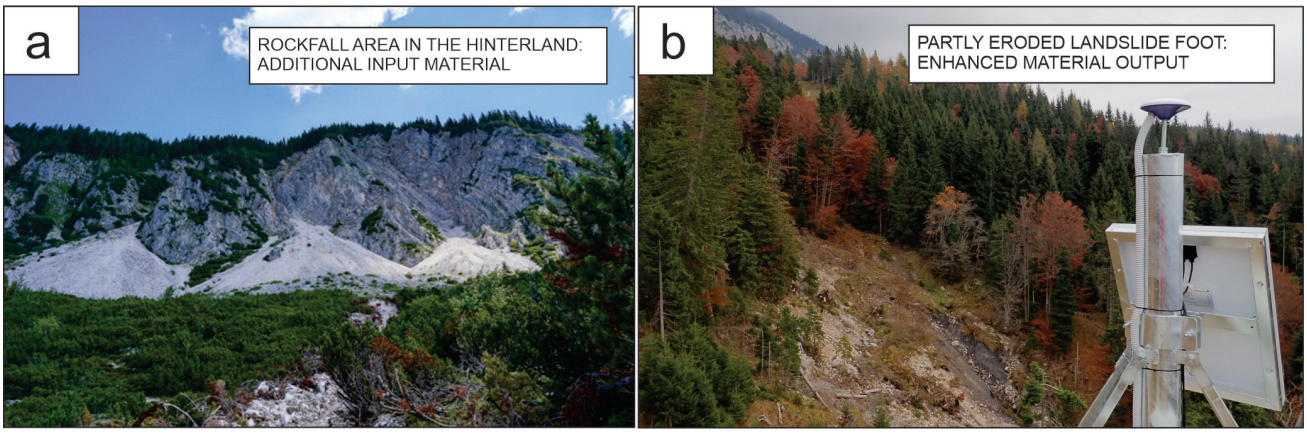

Fig. 3. Field view of specific elements of the composed landslide in the dynamic alpine conditions, an example of Urbas landslide. a – The rockfall input area provides a supplementary sliding material. Past rockfall events that are already vegetated are visible in the front, b – Fluvially eroded landslide foot.

Above the deep-seated landslide body, the area is bounded by the rocky mountain ridge composed of the Triassic and Jurassic limestone. A wide rockfall zone indicates locally tectonized and mechanically weak rocks that with different processes such as rockfalls, rockslides and toppling of boulders, provide a continuous supply of the slope material to the surface of the deep-seated landslide body. The material accumulates under the steep rocky cliffs in a form of several accumulation fans that cover the landslide crown so that the main scarp remains buried underneath, invisible to the naked eye. Traces of inactive, partly vegetated talus cones extending further downslope indicate more intensive rockfall activity in the past (Fig. 3a).

Downslope, the deep-seated landslide body is limited by the geologic contact between weathered clastic and considerably more compact Palaeozoic and Triassic carbonate rocks. There, the two ridges composed of relatively more stable bedrock force the sliding mass accumulating from a 500 m wide area to move through the narrow, 100 m wide debris flow channel (Fig. 3b). The channel was incised by the Bela stream that collects surface waters from the main landslide body characterized by the low permeability of clastic rocks. While the soft clastic rocks are mostly washed out by the Bela stream in a suspension, fragments of different sizes originating from the rockfall zone in the hinterland of the landslide body are gradually, but constantly transported down the Bela stream towards the distant Sava valley. Such topography disables the deposition of a typical landslide foot. Instead, several paleo alluvial sedimentary bodies evidenced in over

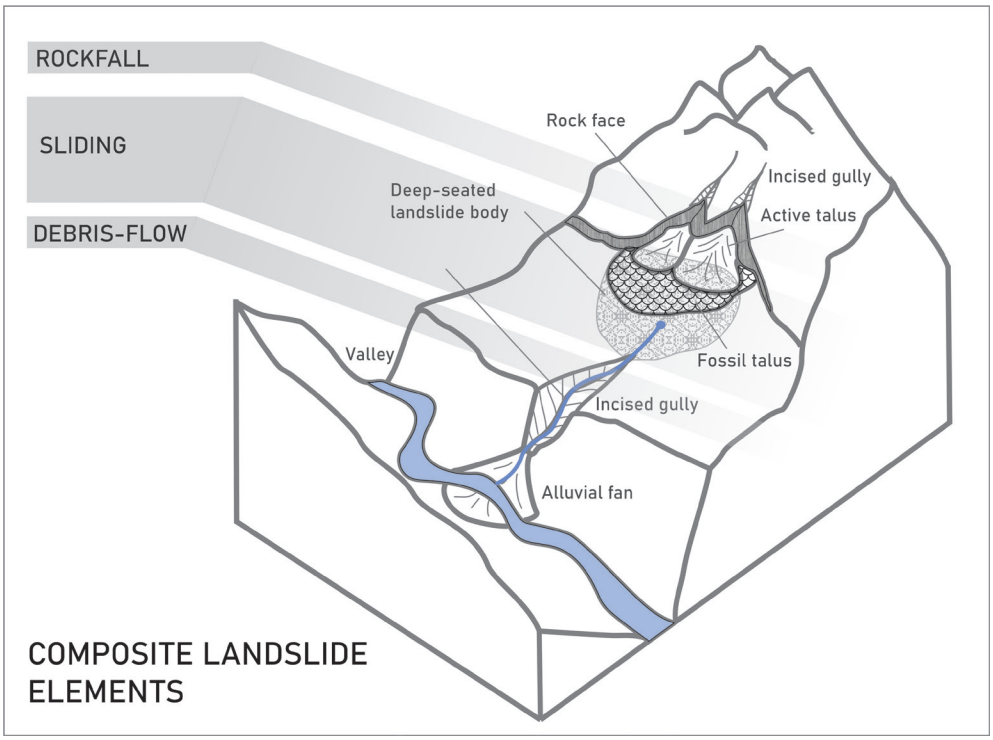

Fig. 4. Composite landslide elements as evidenced in the case study of the Urbas landslide.

2 km distant Sava valley indicate that the material originating from the landslides in the area mobilized into the debris flows during the several massive, instantaneous events (Jež et al., 2008; Jež et al., 2019) (Fig. 1).

Investigations revealed that the Urbas landslide is composite landslide (Cruden & Varnes, 1996) consisting of three elements characterized by different types of movements:

- rockfall area located in the upper part,
- deep-seated landslide defined by the sliding surface, and
- debris-flow source area located in the lower part of the composite landslide (Peternel et al., 2017; Peternel, 2017) (Fig. 4).

For a complete understanding of geomorphological processes operating within the composite landslide, we considered not only the deep-seated landslide defined by its sliding surface but the entire area of the composite landslide phenomena including an active rockfall zone, main deep-seated landslide body, talus accumulation area, the zone of the debris flow channel and surrounding unstable or potentially unstable areas that exhibit shallow surface displacements visible on the digital elevation model (Fig. 2).

Materials and methods

Monitoring techniques

Inaccessibility, lack of electric power, irregular topography, steep slopes, specific slope aspect, extreme weather conditions, dense vegetation, as well as nature protected areas (Natura 2000 etc.) represent common limitations in monitoring complex environments such as the alpine. Such

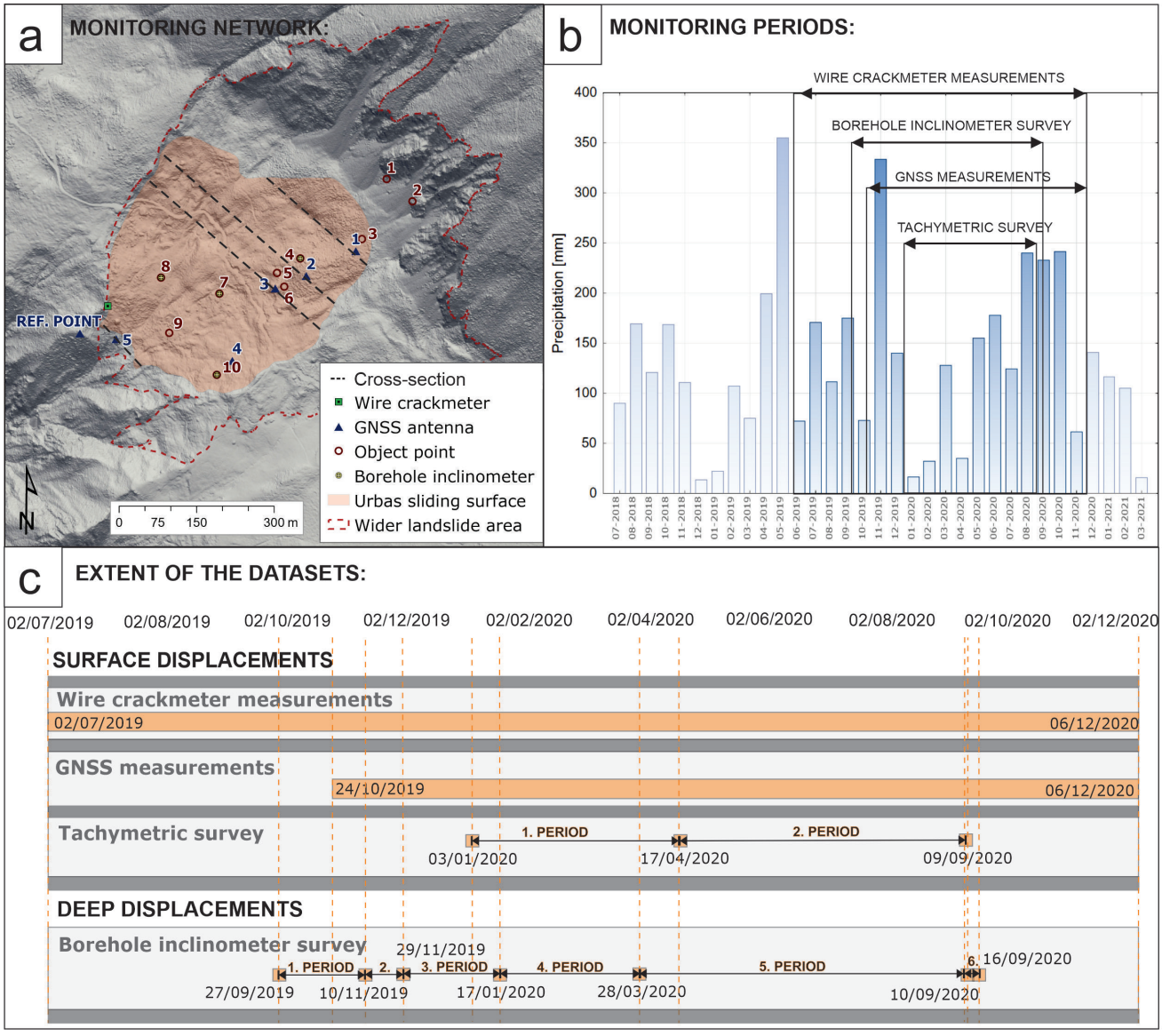

Fig. 5. a – Monitoring network, b – Monthly precipitation values during the monitoring, c – The extent of the integrated datasets.

limitations prevent some monitoring techniques from acquiring satisfactory results, for example, the InSAR. Considering all the constraints, the Urbas landslide was simultaneously monitored with four different monitoring techniques which were considered to deliver the most useful results and were integrated to obtain the complete kinematics of the landslide (Fig. 5a, c). They include two continuous (wire crackmeter and GNSS), and two periodic monitoring techniques (in situ geodetic field campaigns using tachymetric measurements and borehole inclinometer surveys) (Fig. 5a, c).

Wire crackmeter measurements

A wire crackmeter consists of a transducer box which includes the rotary electronic sensor with a wire tensioning device. The target is an eyebolt expansion anchor (Fig. 6a). The wire crackmeter is located at the right flank in the lower part of the Urbas landslide (Fig. 5a). It continuously monitors the opening of the right flank by providing measurements at 15 min intervals. It measures the absolute length of the wire installed across the crack, presuming that the carbonate ridge at the outer side of the scarp is stable. The stability of the ridge was approved by the geological-geomorphological field examination (Peternel et al., 2018). The accuracy of the wire crackmeter measurements is estimated to be 1 mm. The extent of the dataset is 1.5 years (Fig. 5c).

GNSS measurements

GNSS stations monitor the displacements occurring at the surface of the landslide (Fig. 6b). Covering the entire landslide body, the GNSS monitoring network aims to reveal spatial differences in landslide kinematics. GNSS monitoring network consists of 6 GNSS stations, with one representing the local reference point (Fig. 5a). Its stability was determined by computing its position over the whole monitoring period by the absolute positioning (PPP) considering the EU plate motion. Based on this, GNSS position calculation daily provides the coordinates (X, Y and Z) of 5 antennae of interest. Technical specifications of the GNSS monitoring system are presented in Šegina et al. (2020). GNSS method provides continuous data with a daily interval with the accuracy of 1 mm for the horizontal component (X, Y) and 2 mm for the vertical component of the displacement (Z). For the scope of this research, the coordinates displacements were presented as a 3D displacement [mm]. Over a one-year-long dataset was available (Fig. 5c).

Tachymetric surveys using a total station

Tachymetric surveys measured accurate surface displacements. Permanent topographic prisms were installed on the concrete plates that surround the piezometers and inclinometers caps (Fig. 6c). The measurements were taken with the Leica Nova MS50 (angular accuracy 1", distance accuracy 1 mm + 1.5 ppm) and Leica GPH1P

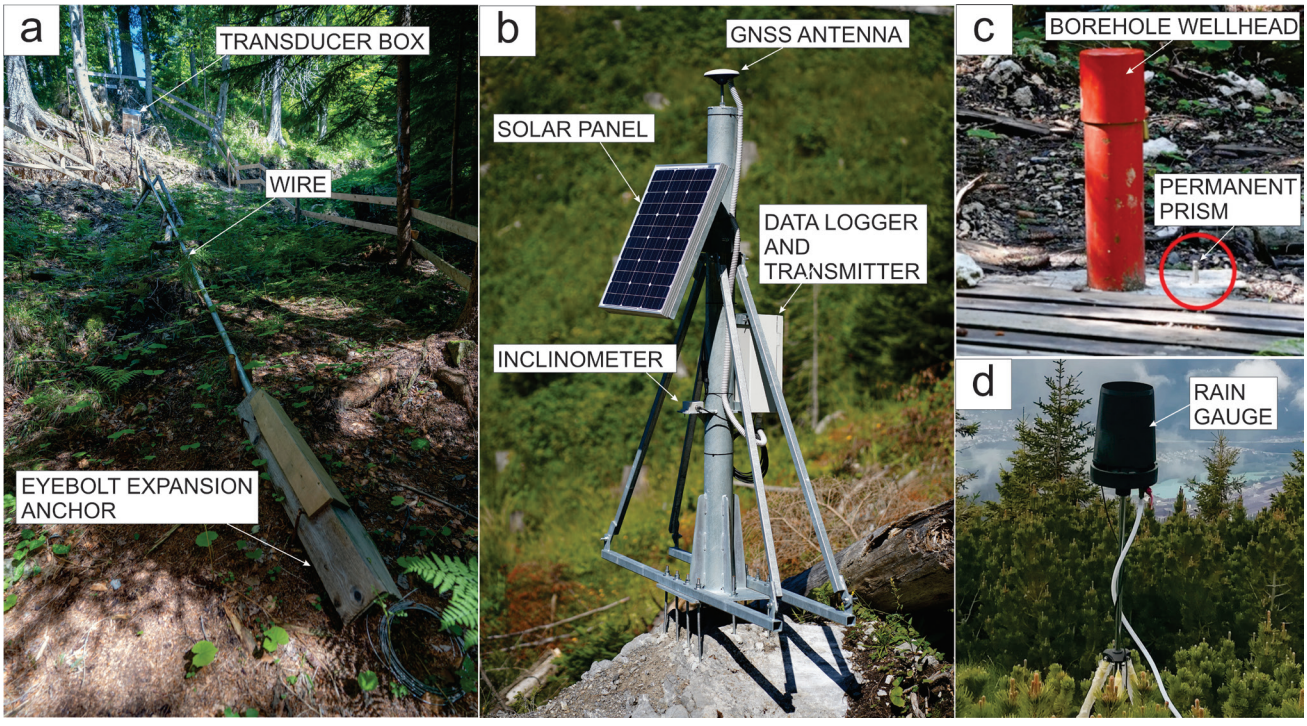

Fig. 6. a – Wire crackmeter, b – GNSS station, c – Location of permanent prisms for a tachymetric survey, d – Rain gauge.

precision prisms (centring accuracy of 0.3 mm). Vertical and horizontal displacements were determined for 8 checkpoints. We established 4 reference points on a supposedly stable terrain (stations 1, 2, 11, and 12 in Fig. 5a). Reference points 11 and 12 are located on the carbonate ridge, which divides the deep-seated landslide body and unstable area on the SE. The displacement were presented as 3D displacements [mm]. Three geodetic field campaigns were carried out in the year 2020 (Fig. 5c).

Borehole inclinometer survey

The borehole inclinometer survey provides unique information on the subsurface landslide displacements down to its sliding surface. A total of four boreholes were drilled and equipped with inclinometer casings with a diameter of 60 mm to define the depth of the sliding surface and to enable monitoring of the displacements of the entire landslide body at various locations. The boreholes were drilled at least 2 m into the stable bedrock to ensure reliable measurements. The measurements were performed down to 34.5 m (Inclinometer 4), 23.5 m (Inclinometer 7), 27.5 m (Inclinometer 8) and 27 m (Inclinometer 10). The horizontal displacements was derived from the tilt of the probe that is measured bottom-up in the borehole with a uniaxial technique and at an interval of 0.5 m. When the probe was unable to pass through the casing, measurements of the absolute shear displacement became impossible (marked with "sheared"). Periodic inclinometer surveys in the boreholes started in September 2019. Seven consecutive borehole inclinometer field measurements were carried out during the years 2019 and 2020 (Fig. 5c).

Precipitation measurements

Rain gauge provides a continuous dataset on the amount of the precipitations with an hourly interval and an accuracy of 0.2 mm. It is located in the central part of the composite landslide area (Fig. 5a and Fig. 6d).

Monitoring data integration

First, we analysed surface and subsurface displacements separately. Subsurface displacements were acquired only with a borehole inclinometer survey. Surface displacements were monitored by three different techniques that were integrated to provide information on the spatial kinematic characteristics of the landslide surface. We integrated two continuous datasets, namely GNSS and wire crackmeter data, with the periodic tachymetric measurements. The integration of continuous and periodic measurements includes the following steps: i) definition of the periods when periodic measurements were acquired, ii) selection of the same periods in the continuous datasets, iii) calculation of absolute displacement that occurred within the defined periods for both datasets and iv) correlation and analysis of the data.

In the next step, we integrated surface and subsurface displacements to analyse landslide kinematic characteristics with depth. We considered surface displacements acquired with a tachymetric survey, wire crackmeter and GNSS methods and subsurface displacements acquired by inclinometer surveys. The integration was carried out following the presented integration method. The displacements data are presented as absolute measured values [mm]. In some cases, the results are presented as average monthly rate [mm/month] to enable the comparison of data in monitoring periods of different duration.

Sediment discharge

Sediment discharge as an indicator of sliding material balance (Guerriero et al., 2017; Mackey et al., 2009) was employed to analyse the interrelationship between the three different elements of the composite landslide. It reveals the potential retention of the material in the area of the deep-seated landslide. The Urbas landslide body is considerably narrowing from the landslide head to the landslide foot due to relatively more stable bedrock that limits the sliding surface from the sides. 500 m wide landslide's head reduces to around 100 m wide valley at the landslide foot (Fig. 2a). To reveal the effect of a decreasing landslide crossection on the displacement rate of the sliding material, we observed the total volume of the displaced material that moved through the sectors of the landslide. Based on the defined sliding surface (Fig. 2b) and the available digital terrain model with 1 m resolution (Slovenian Environmental Agency), we extracted the cross-sections across the landslide at the locations of four GNSS monitoring points (GNSS 1, 2, 3 and 5) that are rather evenly distributed along the profile of the landslide (Fig. 5a).

We calculated the difference between the volume of the material that entered and the volume of the material that left the particular sector (sectors are shown in Fig. 11) between the adjacent GNSS points during the entire GNSS monitoring period (24/10/2019–06/12/2020), assuming that on the cross-section, the landslide moves perpendicular

to it and with same rate as measured with the GNSS method:

$$\Delta V=(A_2 \times d_2) - (A_1 \times d_1) \quad (1)$$

A_1 = *area of the upper cross-section [m²]*
A_2 = *area of the lower cross-section [m²]*
d_1 = *measured displacement at the upper cross-section [m]*
d_2 = *measured displacement at the lower cross-section [m]*

Results and discussion

Surface displacements

Surface displacements were analysed during the period between 03/01/2020–09/09/2020 (251 days). They combined the data acquired with GNSS stations, wire crackmeter and tachymetric surveys (Table 1). To align with tachymetric field campaigns, we isolated two periods, namely the first between 03/01/2020–17/04/2020 (106 days) and the second between 17/04/2020–09/09/2020 (145 days) (Table 1).

Object points 1 and 2 are located on the bedrock that is considered stable. The surface morphology indicates that the left flank of the landslide is not entirely stable, but during the monitoring period, the displacement was small (18.71 mm) (Object point 10), or even under the detectability of the method (GNSS 4). Small displacements were also detected by the wire crackmeter at the right flank of the landslide (23.91 mm). Medium displacements occurred at the landslide head (36.17–46.69 mm) (Object points 3–6 and GNSS 1–3). Similar displacements were observed at Object point 8. Higher activity was observed at the central part of the landslide (Object points 7 and GNSS 5). During the monitoring period, this part moved for approximately 150 mm.

Figure 7a shows a spatial distribution of surface displacements. The most complete dataset shows the displacements measured during the second monitoring period. It visualizes spatial heterogeneity in the kinematics of landslide surface material. At the surface, the central part of the landslide moves considerably faster than on the edges and at the head of the landslide.

Table 1. Measured displacements of the surface material.

PERIOD	03/01/2020 17/04/2020	18/04/2020 09/09/2020	03/01/2020 09/09/2020
DURATION [number of days]	106	146	252
SURFACE DISPLACEMENT [mm]	**DISPLACEMENT IN PERIOD 1 [mm]**	**DISPLACEMENT IN PERIOD 2 [mm]**	**CUMULATIVE DISPLACEMENT [mm]**
Object point 1	0.00	0.00	0.00
Object point 2	0.00	0.00	0.00
Object point 3	15.58	21.51	37.09
Object point 4	19.66	24.42	44.08
Object point 5	21.24	25.45	46.69
Object point 6	17.06	23.86	40.91
Object point 7	69.35	86.17	155.52
Object point 8	19.88	27.52	47.40
Object point 9		73.23	
Object point 10	13.93	4.79	18.71
GNSS 1	13.90	25.82	39.52
GNSS 2	16.29	27.77	43.90
GNSS 3	13.20	23.09	36.17
GNSS 4	under detectability	under detectability	under detectability
GNSS 5	47.96	97.66	145.58
Reference point	0.00	0.00	0.00
Wire crackmeter	9.54	14.37	23.91

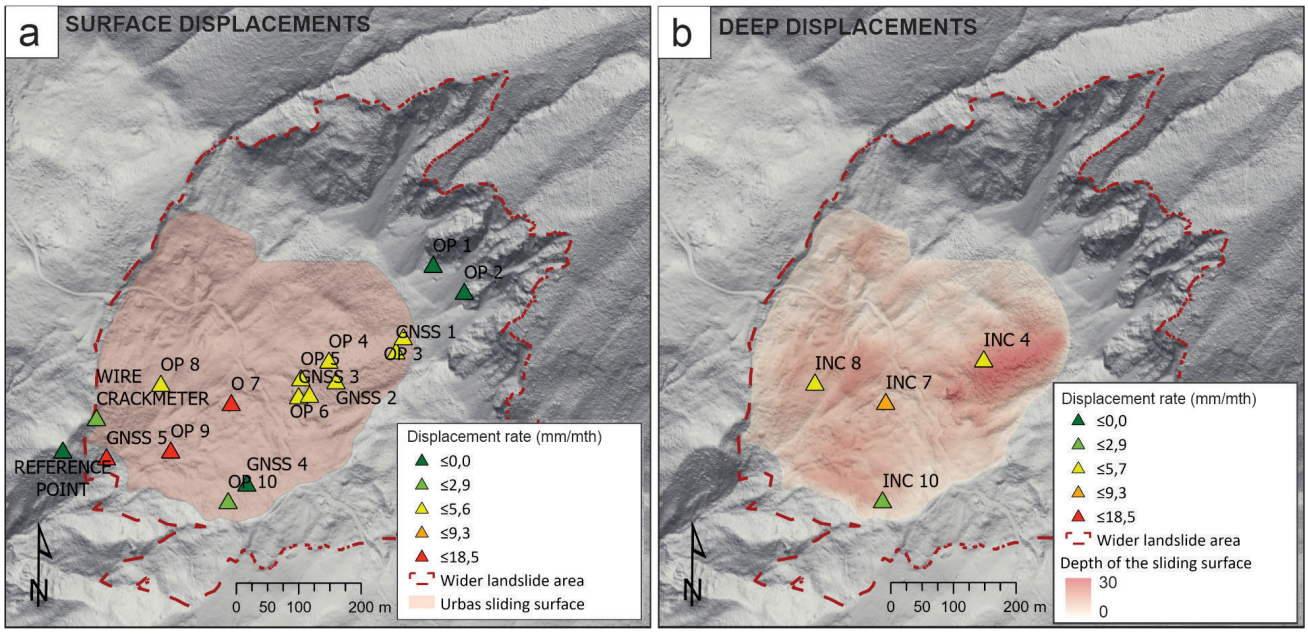

Fig. 7. a – Surface displacement rate measured in the second monitoring period. b – Subsurface displacement rate at the sliding surface and the depth of the sliding surface. Scales are comparable.

Subsurface displacements

The borehole inclinometer survey indicates a variable depth of the sliding surface of the deep-seated landslide body. It occurs down to the depth of 20 m in the central part and at the head of the landslide, at 11.5 m at the right and 3.5 m at the left flank of the landslide. Based on other borehole drillings and geophysical surveys carried out during the investigation of the Urbas landslide, the sliding surface is the deepest at the head of the landslide due to thick deposits of the slope talus, followed by the central part of the landslide (Fig. 7b).

Subsurface displacements were measured in four boreholes during the period between 27/09/2019-16/09/2020 (356 days) (Fig. 5c). Seven borehole inclinometer surveys were carried out during this time. They defined six monitoring periods (Table 2, Table 3). We present results of displacements measured at the depth of 1 and 10 m, respectively. At the depth of 20 m, no displacement occurred in any borehole.

The same spatial heterogeneity of the displacement trends detected at the surface was observed also in the depth of the landslide body (Fig. 7a, b). Generally, similar spatial relationships were observed: the largest subsurface displacement was measured in the central part, medium in the head and minimal at the left flank of the landslide area (Table 2, Table 3, Fig. 7b).

Vertically, the observed displacements indicate various types of movements in different parts of the deep-seated landslide body. Some parts move as a compact sliding mass while some developed several sliding surfaces or exhibit a gradual vertical change in sliding velocity. Such behaviour is related to the geomechanical characteristics of the sliding material and the topography of the sliding surface. At the head of the landslide (Inclinometer 4) and at the right flank

Table 2. Measured displacements at the depth of 1 m.

PERIOD	27/09/2019 10/11/2019	11/11/2019 29/11/2019	30/11/2019 17/01/2020	18/01/2020 28/03/2020	29/03/2020 10/09/2020	11/09/2020 16/09/2020	27/09/2019 16/09/2020
DURATION [number of days]	45	19	49	72	167	6	356
SUBSURFACE DISPLACEMENTS (at -1 m) [mm]	**PERIOD 1 [mm]**	**PERIOD 2 [mm]**	**PERIOD 3 [mm]**	**PERIOD 4 [mm]**	**PERIOD 5 [mm]**	**PERIOD 6 [mm]**	**CUM. DISPL. [mm]**
Inclinometer 4		15.3		10.3	26.4		52.0
Inclinometer 7			47.8	9.3 sheared			57.1
Inclinometer 8	7.6	1.9	11.0	14.0	24.9		59.4
Inclinometer 10		2.6		0.0	0.6		3.2

Table 3. Measured displacements at the depth of 10 m.

PERIOD	27/09/2019 10/11/2019	11/11/2019 29/11/2019	30/11/2019 17/01/2020	18/01/2020 28/03/2020	29/03/2020 10/09/2020	11/09/2020 16/09/2020	27/09/2019 16/09/2020
DURATION [number of days]	45	19	49	72	167	6	356
SUBSURFACE DISPLACEMENTS (at -10 m) [mm]	**PERIOD 1 [mm]**	**PERIOD 2 [mm]**	**PERIOD 3 [mm]**	**PERIOD 4 [mm]**	**PERIOD 5 [mm]**	**PERIOD 6 [mm]**	**CUM. DISPL. [mm]**
Inclinometer 4		16.6		11.3	25.8		53.7
Inclinometer 7			0.00*	sheared			
Inclinometer 8	7.6	2.4	10.7	13.0	24.8		58.5
Inclinometer 10		0.0		0.6	0.2		0.8

* The displacement is not captured because the sliding surface occurs at 9 m.

(Inclinometer 8), the landslide body moved rather homogeneously from the sliding surface up to the topographical surface as a thick layer of gravel (or clayey gravel) slides on tectonically weakened mudstone (Fig. 8). On the opposite, the left flank of the landslide moved heterogeneously, forming two sliding surfaces at 4 and 11.5 m depth respectively (Inclinometer 10) (Fig. 8). The displacements recorded shallower with respect to the sliding surface at -3 m are of anthropogenuous nature. The landslide body moved heterogeneously in the central part as well (Inclinometer 7). In this sector, the rate of displacement with depth gradually decreases due to heterogeneity of the sliding material and irregular basement morphology that cause the material to slow down (Fig. 8). In the 2. period, the inclinometer was sheared due to active sliding processes and further displacement monitoring was impossible (see Table 3). The nature of displacements along the landslide profiles as indicated by the inclinometer measurements indicates translational type of landslide movement.

The interaction of surface and subsurface displacements

We integrated surface displacements acquired with a tachymetric survey at inclinometers caps and subsurface displacements derived from inclinometer measurements. We compared the 1. period of a tachymetric survey (03/01/2020-17/04/2020) with the 4. period of borehole inclinometer survey (17/01/2020-28/03/2020) (common

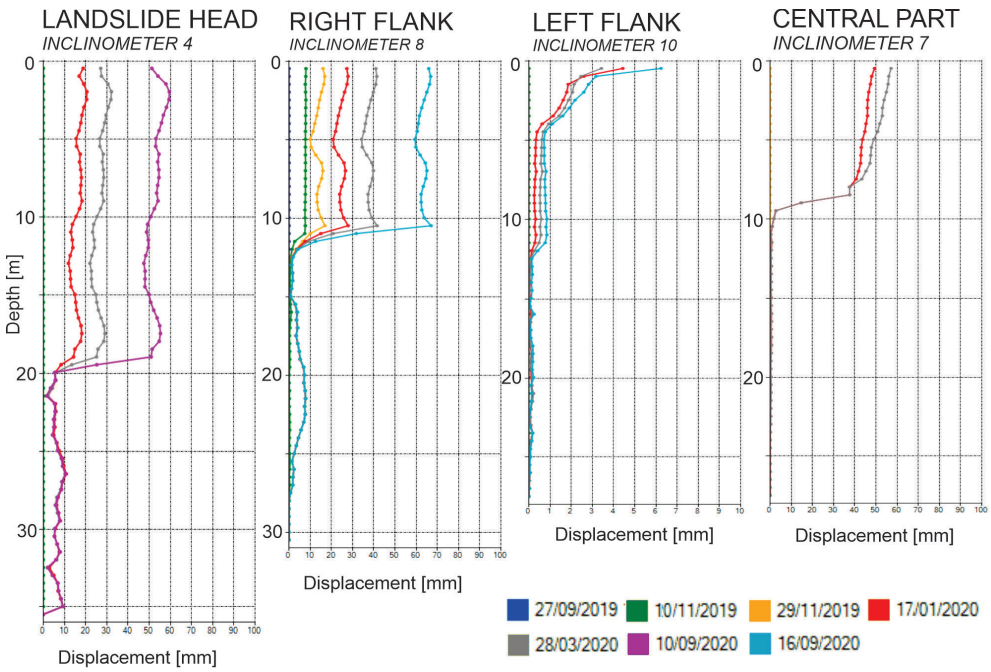

Fig. 8. The characteristics of subsurface displacement: A – at the landslide head (Inclinometer 4), B – at the right flank of the landslide (Inclinometer 8), C – at the left flank of the landslide (Inclinometer 10) and D – in the central part of the landslide (Inclinometer 7).

period 1) and the 2. period of the tachymetric survey (17/04/2020–09/09/2020) with the 5. period of the borehole inclinometer survey (28/03/2020–10/09/2020) (common period 2) (see Fig. 5c). The discrepancy of surface displacements obtained by tachymetric survey in comparison to 1 m and 10 m deep displacements obtained by inclinometer measurements are presumed to be related to a weak temporal overlapping of the observed periods (common period 1: 34 days longer observation period for tachymetric measurements; common period 2: 21 days longer observation for inclinometer measurements) (Fig. 9). Considering this, the surface and deep displacements seem to be relatively homogeneous and the landslide movement can be considered as translational.

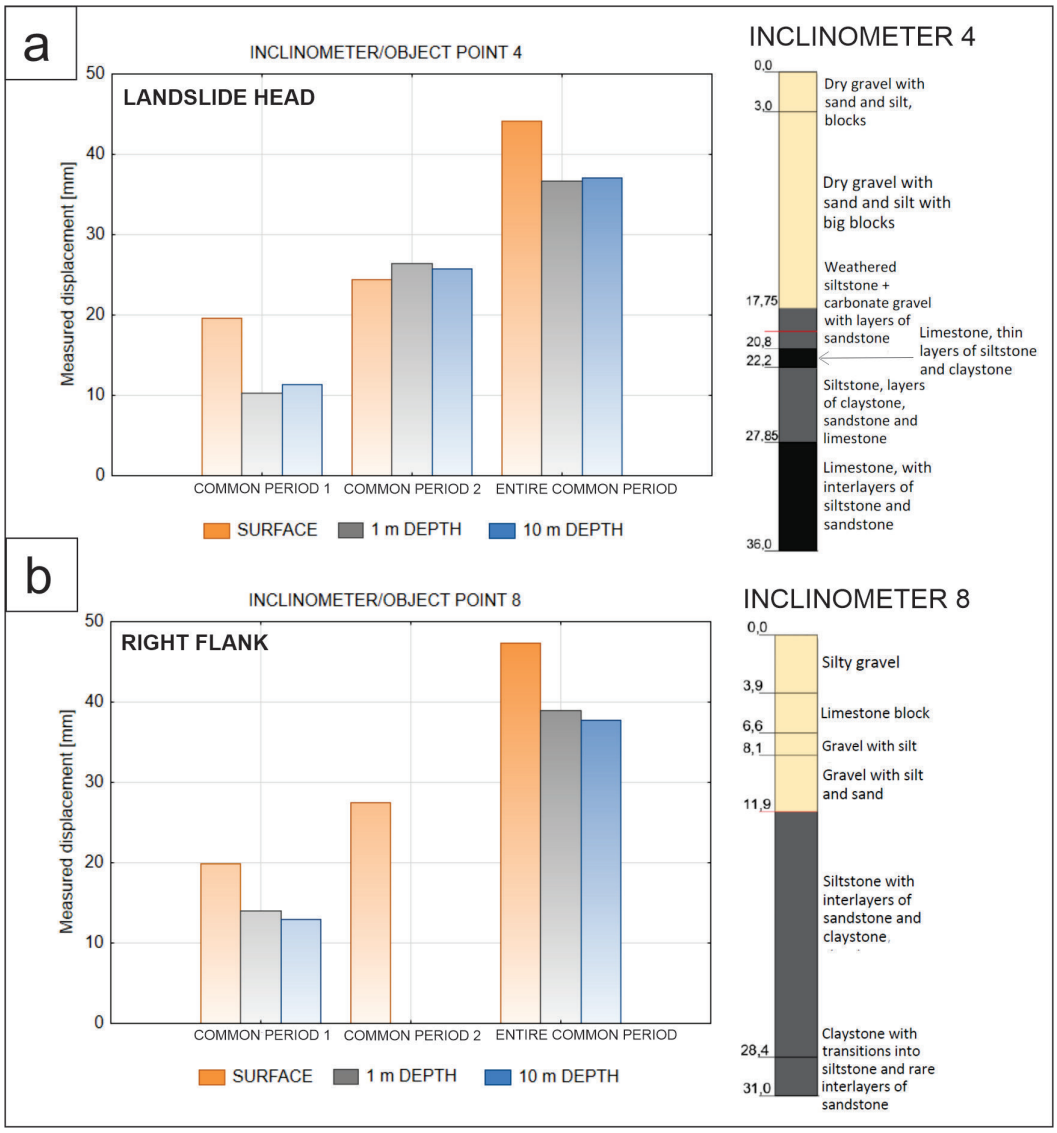

Fig. 9. Combined data on surface and subsurface displacements at the Inclinometers / Object points 4 and 8.

Table 4. Sliding material balance. Sectors are shown in Figure 5 and Figure 10.

SECTOR	Area of cross-section – IN [m²]	Measured displacement – IN [m]	Area of cross-section – OUT [m²]	Measured displacement – OUT [m]	V of displaced material – IN [m³]	V of displaced material – OUT [m³]	ΔV [m³]
UPPER	2417	0.072	4273	0.079	174	338	-164
MIDDLE	4273	0.079	3862	0.069	338	267	71
LOWER	3826	0.069	119	0.570	267	68	199

Sliding material balance

Referring to the vertical kinematic homogeneity, surface displacements obtained by the GNSS method were considered in the calculation of the sliding material balance.

Calculation showed that 164 m³ more material left the upper sector than entered it (Fig. 10). Several explanations are possible: i) we underestimated the extent of the sliding surface in the upper (northern) part of the landslide, ii) the upper part of the landslide is emptying (no morphological signs visible to confirm this option), iii) the upper part of the landslide moves irregularly in time so that the complete kinematic characteristics of the sliding was not captured. Based on the data from the GNSS station recently located in the northern part of the landslide, the sliding surface must had been underestimated in this area.

In the middle and lower sectors, 71 and 199 m³ less material left the areas than entered them respectively, indicating the minor retention of the material in both sectors. The amounts of the retained material are relatively small, but only over a year-long monitoring period has been considered.

Bottom line, 270 m³ of the sliding material retained in the middle and lower sectors of the landslide. More reasonably, monitoring at the landslide foot does not entirely capture the displacement of the output material, as soft rocks are washed out in a suspension and unconsolidated scree material of small dimensions probably moves faster than fragments of a size of a boulder on which GNSS 5 is installed. Thus, the actual volume that retained on the landslide is presumably considerably smaller than calculated. Also, the calculations consider rather a short monitoring period (one year and 2 months) which might not be enough to reveal the complete sliding material balance.

Kinematics of the composite landslide Urbas

A deep-seated landslide body moves rather homogeneously, indicating the translational type of the landslide movement. Current data suggest that the displacement at the sliding surface is induced by the scree accumulation which poses an additional load on the uppermost part of the deep-seated landslide body. However, an additional hydrological analysis will give a clearer insight into the triggering factors of the displacement mechanisms in the head of the deep-seated landslide.

Sediment discharge indicates no substantial accumulation of the material in the area of the landslide. At present conditions, the composite landslide Urbas is a rather balanced geomorphic system, where the supplementary input of the material from the rockfall zone is rather successfully compensated with the enhanced erosion of the material in the debris-flow channel at the landslide foot. The increased displacement rate evidenced in the area of eroded landslide foot mainly reflects the topographical narrowing of the space available for the transport of the material through the debris-flow channel rather than incrised activity of the sliding in this part. The localised erosion in this part of the composite landslide is particularly effective due to the low permeability of the bedrock in the main landslide body that provides temporary and permanent streams. However, the evidence of past events indicates that, in particular weather conditions, the occasional extreme debris-flow events are capable of reaching the bottom of the valley (Jež et al., 2008).

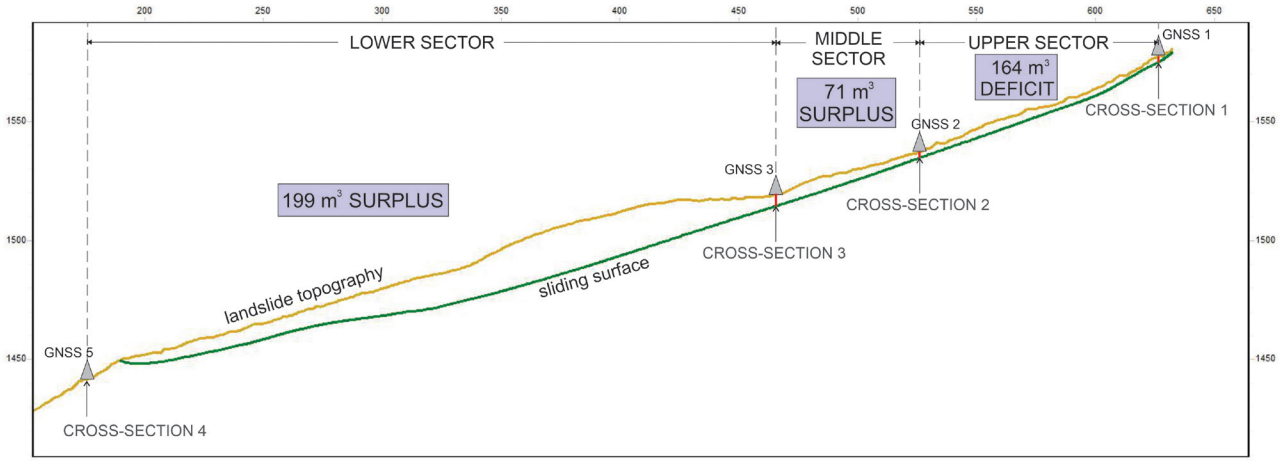

Fig. 10. Sliding material balance along the longitudinal profile of the landslide. The SKUA-GOCAD software was used to obtain the main sliding surface.

Conclusions

Due to complex geology and terrain topography, the alpine areas are common environments for landslide formation. This research shows that rather than simple sliding, specific environmental settings induce the formation of composite landslides characterized by several simultaneous and interacting types of movements. Understanding such landslide kinematics requires a comprehensive approach including the following elements:

- the definition of the complete landslide area that includes, together with the landslide body defined by its sliding surface, also the potential material supply and erosion zones,
- extended monitoring network capable of capturing the spatial differences of the displacement trends,
- consideration of both surface and subsurface displacements,
- consideration of the dynamic sliding system: a constant supply of the additional material from the rockfall areas in the hinterland, representing continuous additional material input, and erosion of the landslide's foot, representing enhanced material output,
- influence of complex geology and topography characteristic for compressional orogens, on landslide kinematics
- estimation of the sliding material balance based on the sediment discharge which considers the topographic aspect of the sliding surface and estimates the potential retention of the material on the landslide area that may represent the potential risk for the occurrence of mass movement events of larger scales.

Acknowledgements

The research was funded by the Slovenian Research Agency (Research Program P1-0419, J1-8153 project; Z1-2638 project, Research Project J1-3024), the Ministry of Environment and Spatial Planning, and the Municipality of Jesenice. We also thank the GIMS project (the European GNSS Agency under the European Union's Horizon 2020 research and innovation programme under grant agreement No. 776335).

References

Baldi, P., Cenni, N., Fabris, M. & Zanutta, A. 2008: Kinematics of a landslide derived from archival photogrammetry and GPS data. Geomorphology, 102:435-444. https://doi.org/doi.org/10.1016/j.geomorph.2008.04.027

Barth, N. 2013: The Cascade rock avalanche: Implications of a very large Alpine Fault-triggered failure, New Zealand. Landslides, 11. https://doi.org/10.1007/s10346-013-0389-1

Baum, R.L., Fleming, R.W. & Johnson, A.M. 1993: Kinematics of the Aspen Grove landslide, Ephraim Canyon, Central Utah. U.S. Geological Survey Bulletin, 1842-F.

Boniello, M. A., Calligaris, C., Lapasin, R. & Zini, L. 2010: Rheological investigation and simulation of a debris-flow event in the Fella watershed. Nat. hazards earth syst. sci., 10/5: 989–997. https://doi.org/10.5194/nhess-10-989-2010

Brückl, E., Brunner, F.K. & Kraus, K. 2006: Kinematics of a deep-seated landslide derived from photogrammetric, GPS and geophysical data. Eng. Geol., 88: 149–159. https://doi.org/10.1016/j.enggeo.2006.09.004

Coe, J.A., Ellis, W.L., Godt, J.W., Savage, W.Z., Savage, J.E., Michael, J.A., Kibler, J.D., Powers, P.S., Lidke, D.J. & Debray, S. 2003: Seasonal movement of the Slumgullion landslide determined from Global Positioning System surveys and field instrumentation, July 1998–March 2002. Eng. Geol., 68: 67-101. https://doi.org/10.1016/S0013-7952(02)00199-0

Crippa, C. & Agliardi, F. 2021: Practical Estimation of Landslide Kinematics Using PSI Data. Geosciences, 11/ 214. https://doi.org/10.3390/geosciences11050214

Crosta, G., Chen, H. & Lee, C. F. 2004: Replay of the 1987 Val Pola Landslide, Italian Alps. Geomorphology, 60: 127-146. https://doi.org/10.1016/j.geomorph.2003.07.015

Cruden, D. & Varnes, D. 1996: Landslides: investigation and mitigation. Chapter 3 - Landslide types and processes. Transportation Research Board Special Report, National Agency of Sciences, Special Report, 247: 36-75.

Fodor L., Jelen M., Márton E., Skaberne D., Čar J. & Vrabec, M. 1998: Miocene-Pliocene tectonic evolution of the Periadriatic line in Slovenia – implications for Alpine-Carpathian extrusion models. Tectonics 17: 690–709.

Frattini, P., Crosta, G.B., Rossini, M. & Allievi, J. 2018: Activity and kinematic behaviour of deep-seated landslides from PS-InSAR displacement rate measurements. Landslides, 15:1053–1070. https://doi.org/10.1007/s10346-017-0940-6

Giordan, D., Allasia, P., Manconi, A., Baldo, M., Satangelo, M., Cardinali, M., Corazza,

A., Albanese, V., Lollino, G. & Guzzetti, F. 2013: Morphological and kinematic evolution of a large earthflow: the Montaguto landslide, southern Italy. Geomorphology, 187: 61–79. https://doi.org/10.1016/j.geomorph.2012.12.035

Gullà, G., Peduto, D., Borrelli, L., Antronico, L. & Fornaro, G. 2016: Geometric and kinematic characterization of landslides affecting urban areas: the Lungro case study (Calabria, Southern Italy). Landslides, 14. https://doi.org/10.1007/s10346-015-0676-0

Guerriero, L., Coe, J. A., Revellino, P., Grelle, G., Pinto, F. & Guadagno, F.M. 2014: Influence of slip-surface geometry on earth-flow deformation, Montaguto earth flow, southern Italy. Geomorphology, 219: 285–305. https://doi.org/10.1016/j.geomorph.2014.04.039

Handwerger, A.L., Roering, J.J., Schmidt, D.A. & Rempel, A.W. 2015: Kinematics of earthflows in the Northern California Coast Ranges using satellite interferometry. Geomorphology, 246: 321–333. https://doi.org/10.1016/j.geomorph.2015.06.003

Hussin, H.Y., Ciurean, R., Frigerio, S., Marcato, G., Calligaris, C., Reichenbach, P., Van Westen, C.J. & Glade, T. 2015: Assessing the effect of mitigation measures on landslide hazard using 2D numerical runout modelling. Landslide Science for a safer geoenvironment, 2: 679–684.

Janža, M., Serianz, L., Šram, D. & Klasinc, M. 2018: Hydrogeological Investigation of Landslides Urbas and ČIkla Above the Settlement of Koroška Bela. Geologija, 61/2:191–203. https://doi.org/10.5474/geologija.2018.013

Jemec Auflič, M., Jež, J., Popit, T., Košir, A., Maček, M., Logar, J., Petkovšek, A., Mikoš M., Calligaris, C., Boccali, C., Zini, L., Reitner, J. & Verbovšek, T. 2017: The variety of landslide forms in Slovenia and its immediate NW surroundings. Landslides, 14. https://doi.org/10.1007/s10346-017-0848-1

Jež, J., Mikoš, M., Trajanova, M., Kumelj, Š., Budkovič, T. & Bavec, M. 2008: Vršaj Koroška Bela - rezultat katastrofičnih pobočnih dogodkov = Koroška Bela alluvial fan - the result of the catastrophic slope events (Karavanke Mountains, NW Slovenia). Geologija, 51/2: 219–227. https://doi.org/10.5474/geologija.2008.022

Jež, J., Peternel, T., Milanič, B., Markelj, A., Novak, M., Celarc, B., Janža, M. & Jemec Auflič, M. 2019: Čikla landslide in Karavanke Mts. (NW Slovenia). In: Uljarević, M., Zekan, S. Salković, S. & Ibrahimović, D. (eds.): Proceedings of the 4th Regional Symposium on Landslides in the Adriatic - Balkan Region. 23-25 Ocober 2019, Sarajevo: Geotechnical Society of Bosnia and Herzegovina: 239–242.

Komac, M., Holley, R., Mahapatra, P., Van Der Marel, H. & Bavec, M. 2014: Coupling of GPS/GNSS and Radar Interferometric Data for a 3D Surface Displacement Monitoring of Landslides. Landslides, 12: 241–257. https://doi.org/10.1007/s10346-014-0482-0

Mackey, B. & Roering, J. 2009: Long-term kinematics and sediment flux of an active earthflow, Eel River, California. Geology, 37: 803–806. https://doi.org/10.1130/G30136A.1

Mikoš, M., Bavec, M., Budkovič, T., Durjava, D., Hribernik, K., Jež, J., Klabus, A., Komac, M., Krivic, M., Kumelj, Š., Maček, M., Mahne, M., Novak, M., Otrin, J., Petje, U., Petkovšek, A., Ribičič, M., Sodnik, J., Šinigoj, J. & Trajanova, M. 2008: Ocena ogroženosti zaradi delovanja drobirskih tokov: končno poročilo: (ciljni raziskovalni projekt: znanje za varnost in mir 2006-2010). Fakulteta za gradbeništvo in geodezijo in Geološki zavod Slovenije, Ljubljana: 224 p.

Mikoš, M. 2020: After 2000 Stože landslide: part I - development in landslide research in Slovenia. Acta hydrotechnical, 33/59: 129–153. https://doi.org/10.15292/acta.hydro.2020.09

Mikoš, M. 2021: After 2000 Stože landslide: part II – development of landslide disaster risk reduction policy in Slovenia. Acta hydrotechnical, 34/60: 39–59. https://doi.org/10.15292/acta.hydro.2021.04

Mikoš, M., Brilly, M., Fazarinc, R. & Ribičič, M. 2006: Strug landslide in W Slovenia: A complex multi-process phenomenon. Engineering Geology, 83/1–3: 22–35. https://doi.org/10.1016/j.enggeo.2005.06.037

Oven, D., Levanič, T., Jež, J. & Kobal, M. 2019: Reconstruction of landslide activity using dendrogeomorphological analysis in the Karavanke mountains in NW Slovenia. Forests, 10/11: article 1009. https://doi.org/10.3390/f10111009

Peternel, T., Jež, J., Milanič, B., Markelj, A. & Auflič, M.J. 2018: Engineering-Geological Conditions of Landslides Above the Settlement of KorošKa Bela. Geologija, 61/2:177–189. https://doi.org/10.5474/geologija.2018.012

Peternel, T. 2017: Dinamika pobočnih masnih premikov na območju Potoške planine z uporabo rezultatov daljinskih in terestričnih geodetskih opazovanj ter in-situ meritev.

Dissertation. Univerza v Ljubljani, Ljubljana: 183 p.

Peternel, T., Jež, J., Milanič, B., Markelj, A., Jemec Auflič, M., Kumelj, Š., Celarc, B., Novak, M., Janža, M. & Šram, D. 2017: Izvedba najnujnejših inženirskogeoloških, hidrogeoloških, geofizikalnih in geomehanskih ter geodetskih raziskav za ugotovitev objektivne stopnje tveganja za prebivalstvo zaradi masnih premikov na območju Potoške planine in izdelava strokovnih podlag s predlogi zaščitnih ukrepov. Geološki zavod Slovenije.

Peternel, T., Šegina, E., Jež, J., Jemec Auflič, M., Janža, M., Logar, J., Mikoš, M. & Bavec, M. 2022: Review of research and evolution of landslides in the hinterland of Koroška Bela settlement in NW Slovenia. Geologija, 62/2: 129–147. https://doi.org/10.5474/geologija.2022.008

Schlögel, R., Malet, J.P., Remaître, A., Reichenbach, P. & Doubre, C. 2015a: Analysis of a landslide multi-date inventory in a complex mountain landscape: The Ubaye valley case study. Natural Hazards and Earth System Sciences Discussions, 3: 2051–2098. https://doi.org/10.5194/nhessd-3-2051-2015

Schlögel, R. Malet, J.P., Doubre, C. & Lebourg, T. 2015b: Structural control on the kinematics of the deep-seated La Clapière landslide revealed by L-band InSAR observations. Landslides, 13. https://doi.org/10.1007/s10346-015-0623-0

Schulz, W.H., Coe, J.A., Shurtleff, B.L., Panosky, J., Farina, P., Ricci, P.P. & Barsacchi, G. 2012: Kinematics of the Slumgullion landslide revealed by ground-based InSAR surveys. In: Eberhardt, E., Froese, C., Turner, A.K. & Leroueil, S. (eds.): Landslides and Engineered Slopes, Protecting Society Through Improved Understanding. 2. Taylor & Francis Group, London, 1273–1279.

Schulz, W. H., Coe, J. A., Ricci, P. P., Smoczyk, G. M., Shurtleff, B. L. & Panosky, J. 2017: Landslide kinematics and their potential controls from hourly to decadal timescales: Insights from integrating ground-based InSAR measurements with structural maps and long-term monitoring data. Geomorphology, 285: 121–136. https://doi.org/10.1016/j.geomorph.2017.02.011

Šegina, E., Peternel, T., Urbančič, T., Realini, E., Zupan, M., Jež, J., Caldera, S., Gatti, A., Tagliaferro, G., Consoli, A., González, J. & Jemec Auflič, M. 2020: Monitoring Surface Displacement of a Deep-Seated Landslide by a Low-Cost and near Real-Time GNSS System. Remote Sensing, 12/20: 3375. https://doi.org/10.3390/rs12203375

Uzielli, M., Catani, F., Tofani, V. & Casagli, N. 2015: Risk analysis for the Ancona landslide - I: characterization of landslide kinematics. Landslides 12: 69–82. https://doi.org/10.1007/s10346-014-0474-0

Varnes, D. 1978: Slope movement types and processes. Transportation Research Board Special Report.

Viganò, A., Rossato, S., Martin, S., Ivy-Ochs, S., Zampieri, D., Rigo, M. & Monegato, G. 2021: Large landslides in the Alpine valleys of the Giudicarie and Schio-Vicenza tectonic domains (NE Italy). Journal of Maps, 17/3: 197–208. https://doi.org/10.1080/17445647.2021.1880979